agriculture

MDPI

Article

Study on Mechanical Properties of Tomatoes for the End-Effector Design of the Harvesting Robot

Shuhe Zheng [1,2], Minglei He [1,2], Xuexin Jia [1,2], Zebin Zheng [1,2], Xinhui Wu [1,2] and Wuxiong Weng [1,2,*]

[1] College of Mechanical and Electrical Engineering, Fujian Agriculture and Forestry University, Fuzhou 350002, China; zsh@fafu.edu.cn (S.Z.)
[2] Fujian University Engineering Research Center for Modern Agricultural Equipment, Fujian Agriculture and Forestry University, Fuzhou 350002, China
* Correspondence: wwx@fafu.edu.cn; Tel.: +86-0591-8375-6227

Abstract: Agricultural robotics has emerged as a research area within robotics, with a particular focus on designing end effectors that are adapted to the physical characteristics of the target fruits. Acquiring a comprehensive understanding of the physical and mechanical properties specific to tomato fruits not only minimizes mechanical damage during grasping processes but also serves as a foundation for the optimal design of gripping components. In this study, the Syngenta Sibede variety of tomatoes was used as the experimental material. The reversible viscoelastic behavior and deformation characteristics of tomato fruits were approximated using a four-element Burgers model through creep testing. The fitting coefficients for the model exceeded 0.99. The creep parameters for the four ripening stages of tomatoes were obtained, and the correlation between the ripening stage, deformation value, and creep parameters was analyzed. Correlation analysis was performed to examine the relationships between each parameter and creep deformation, revealing significant and highly significant correlations. Inter-parameter correlations were also found to be highly significant. Puncture tests were conducted on tomatoes. The exocarp rupture force of the green-ripening stage was 9.224 ± 0.901 N, which was 53.87%, 70.63%, and 104.01% higher than that of the semi-ripening stage, early firm-ripening stage, and mid-late firm-ripening stage, respectively. This study suggests that when harvesting tomatoes at the semi-ripening stage and beyond, attention should be paid to trimming the stem. Compression experiments were conducted on tomatoes, and it was discovered that under the same ripening stage, the axial compressive rupture force of tomatoes was greater than the radial rupture force. Tomatoes exhibited anisotropic behavior. The grasping direction is axial, which can be used as the new design direction of the end-effector.

Keywords: tomato; maturity; viscoelastic behavior; Burgers model; experiment

check for updates

Citation: Zheng, S.; He, M.; Jia, X.; Zheng, Z.; Wu, X.; Weng, W. Study on Mechanical Properties of Tomatoes for the End-Effector Design of the Harvesting Robot. *Agriculture* **2023**, *13*, 2201. https://doi.org/10.3390/agriculture13122201

Received: 9 October 2023
Revised: 14 November 2023
Accepted: 20 November 2023
Published: 26 November 2023

Copyright: © 2023 by the authors. Licensee MDPI, Basel, Switzerland. This article is an open access article distributed under the terms and conditions of the Creative Commons Attribution (CC BY) license (https://creativecommons.org/licenses/by/4.0/).

1. Introduction

The tomato, a fruit-bearing vegetable of the Solanaceae family, is widely cultivated across the globe due to its exceptional nutritional value. Currently, China holds the title of the world's largest producer of tomatoes, according to statistical data from the Food and Agriculture Organization of the United Nations (FAO) database. In 2020, China cultivated tomatoes on 1.1115 million hectares of land, producing an exceptional output of 64.8658 million metric tons. These figures equate to around 22.00% and 34.72% of global production, respectively [1–3]. The majority of tomato harvesting in China is carried out manually, which constitutes roughly 50–60% of total production costs. Manual harvesting, grading, and packaging procedures are not only complicated and ineffective but also prone to causing damage to the fruit during handling, which ultimately affects the quality of tomatoes [4–7]. Agricultural robotics has emerged as a novel research direction within greenhouse environments, with improved controllability compared to outdoor cultivation. Specifically, tomato harvesting and associated tasks such as grading and packaging require

tomato harvesting robots to perform two fundamental actions, gripping and detachment, both of which necessitate precise force application. These robots often use end-effectors to apply force directly to the tomato for stable grasping and to perform actions such as stem cutting, twisting, and snapping. Due to tomatoes being viscoelastic, it is important to understand their physical and mechanical properties. These properties not only mitigate mechanical damage during the gripping process but also provide a foundation for the design of effective grasping components [8–10].

Numerous scholars, both domestically and internationally, have conducted mechanical experiments on tomatoes. Zhou et al. [11] constructed an artificial neural network model to estimate tomato viscoelastic parameters through a creep test and utilized the parameters estimated within the initial 0.2 s to calculate the range of gripping forces for robots. Wang et al. [12], after conducting mechanical tests on tomato stems, determined the mechanical properties of stem sections. They identified a hard rubber material with a thickness of 13 mm and a Shore hardness of 68.2 as suitable for the clamping mechanism, allowing for the safe detachment of lateral branches from the abscission zone. Ince et al. [13], using the Jadelo F1 tomato variety, studied the impact of ripeness on structural mechanical properties through compression and puncture tests. Their findings demonstrated that the a*/b* color parameter was a good indicator for the changing of the mechanical properties. When the firmness values varied between 1.55 N/mm and 2 N/mm, the tomato reached the breaker and turning-color stages and could be harvested easily. Zhang et al. [14] conducted creep tests on early and mid-ripping stage tomatoes and obtained viscoelastic parameters using the Burger model. They determined variable deceleration to be the optimal gripping mode. Numerous scholars, both domestically and internationally, have conducted mechanical experiments on various types of fruits and vegetables. Pham et al. [15] investigated the texture and mechanical properties of Fengshui pear and Shingo pear through a double-bite compression test, aiming for a comprehensive understanding of these attributes. They found that the strain at fracture of Shingo pear is 70% higher than that of Fengshui, and the stress of Shingo at fracture is three times higher than that of Fengshui. Stropek Z et al. [16,17] proposed a method for calculating the plastic deformation energy and analyzed the deformation energy of apples and pears under impact loads. Shirvani M et al. [18] used the Boussinesq, Hooke, and Hertz theories to determine the elastic modulus of three apple varieties. The results of this experiment showed that the Golden Delicious variety had the lowest modulus of elasticity (2.211 MPa) while the Granny Smith variety showed the highest modulus of elasticity value (3.431 MPa). They concluded that the Hertz theory is more applicable to intact apple samples. Bi et al. [19] used creep recovery analysis to investigate the viscoelasticity of soy protein isolate, discussing the flexibility, rigidity, and viscosity of SPI molecules concerning creep time, shear stress, and creep temperature. Chen et al. [20] used dynamic mechanical analysis (DMA) for temperature scanning, frequency scanning, stress relaxation, and creep tests on husked barley stems with varying moisture content (10.23–43.14%). The results indicated significant dependence of storage modulus, loss modulus, and tangent delta on moisture content. Hou et al. [21] summarized the impact, vibration, and static pressure mechanical damage characteristics of various berries, stone fruits, pome fruits, citrus fruits, and nuts. They found that mechanical damage caused by impact and vibration mainly occurred during harvesting, while damage from static pressure predominantly happened during storage and transportation. Among impact characteristics, impact height, angle, and material of the fruit plate had substantial effects on fruit damage. Jahanbakhshi et al. [22] studied the mechanical properties of bananas, revealing that the maximum forces required for bruising, bending, and shearing banana fruit were 194 N, 46.26 N, and 48.06 N, respectively. To minimize mechanical damage, the pressure generated during product conveyance must be reduced to the lowest possible rate (below 194 N). Wu et al. [23] conducted creep tests on watermelon stems, extracting their viscoelastic parameters.

With the development of harvesting robots, domestic and international research on end-effectors tends to diversify. Vu et al. [24] designed a four-finger gripping end-effector

for tomato harvesting. The end-effector combines a gripper with a vacuum nozzle that can move simultaneously with the fingers. Jun et al. [25] developed a tomato harvesting end-effector. The proposed soft material suction gripper creates a pressure difference between the inner and outer surfaces, which enables the gripping of tomatoes. The cutting module consists of a pair of scissors and a matching rotating scissor blade. The fluid variable pressure end-effector is also the current mainstream development direction, which usually acts on the surface of the fruit, the fruit envelope, and is later separated by pulling off or twisting off the fruit stalk. Deimel et al. [26] created a flexible manipulator with an excellent payload-to-weight ratio, which can lift almost three times the weight of the object.

In contemporary research papers, many mechanical experiments on tomatoes disregard the impact that end-effector design may have on them. Additionally, there is a lack of requirements or suggestions for the design of the end-effector. One significant challenge in the development of tomato-picking robots is the insufficient handling of pedicel cutting. Incomplete cutting can result in excessively long pedicels, which may injure neighboring fruits during storage and shipping. This surface damage can permit fungal intrusion, resulting in decay and spoilage of the tomatoes. To fully understand the physical and mechanical properties of tomato fruits, minimize mechanical damage during gripping, and provide technical support for the optimization of end-effector gripping components. In this study, three experiments were carried out, as shown in Figure 1: (1) By conducting puncture tests to mimic the insertion of the tomato pedicel, the mechanism of puncture damage was elucidated. The rupture force of tomato exocarp at different stages of ripeness was examined, leading to the identification of ripening stages where the need for pedicel trimming was more pronounced; (2) Most harvesting robots adopt operation modes such as grip–cut or grip–twist, both of which inherently involve clamping the tomato. Tomato deformation during gripping was simulated using creep tests, providing guidance for reducing damage during tomato grasping and informing the design of gripping components; (3) This study revealed the mechanism of tomato rupture under compression through compression test. By subjecting tomatoes to both radial and axial compression, it was investigated whether tomatoes exhibited anisotropy and vulnerable areas.

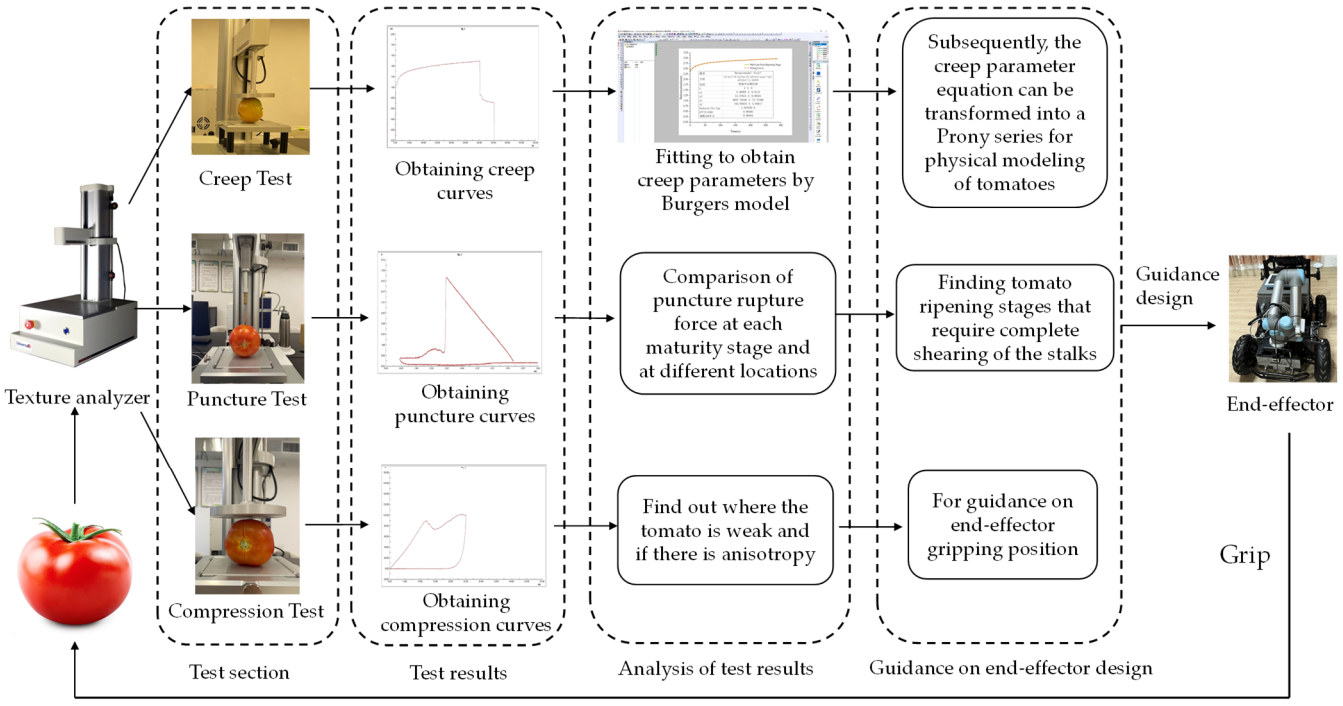


Figure 1. Tomato mechanical properties test.

2. Materials and Methods

2.1. Sample Preparation

The tomatoes used for experiments in this study were selected and harvested, assessed with the naked eye, based on the color of the tomatoes in a plastic film greenhouse at the Yinong Agricultural Base in Changle District, Fuzhou City, Fujian Province, China. The greenhouse is located at 119.47° E and 25.91° N, with an altitude of 4 m. These tomatoes were planted in March and ripened successively from May to July. All tomatoes were free from deformation, scarring, pests, or damage. All tomatoes were stored under laboratory conditions for one day before starting this experiment. The physical parameters of the tomato samples are shown in Table 1. Fourteen tomatoes in each maturity group were numbered, and their diameter, minor diameter, height, and weight were measured using a digital vernier caliper (Deli Group Co., Ltd., Ningbo, China) (Accuracy: 0.01 mm) and sensitive scale (Sartorius (Shanghai) Trading Co., Ltd., Shanghai, China) (Accuracy: 0.001 g).

Table 1. The physical parameters of the tomato samples.

Physical Parameters		Green-Ripening Stage	Semi-Ripening Stage	Early Firm-Ripening Stage	Mid-Late Firm-Ripening Stage
Diameter (mm)	Max	80.21	72.04	86.86	83.29
	Mean	70.73 ± 6.18	65.83 ± 4.30	72.15 ± 8.11	71.70 ± 6.69
	Min	63.27	60.04	57.25	59.11
Minor Diameter (mm)	Max	76.92	69.95	84.45	78.98
	Mean	66.63 ± 6.78	63.78 ± 3.74	69.39 ± 7.65	68.54 ± 5.63
	Min	58.44	57.42	54.69	58.34
Height (mm)	Max	65.51	71.11	112.43	132.61
	Mean	57.86 ± 4.74	61.77 ± 4.87	57.00 ± 3.12	62.07 ± 20.44
	Min	51.38	55.04	51.35	52.90
Weight (g)	Max	225.496	202.448	252.640	228.865
	Mean	154.116 ± 41.599	151.347 ± 24.799	167.489 ± 43.937	156.586 ± 44.144
	Min	110.203	111.379	88.299	55.160
Quantities		14	14	14	14

Consumer demand for tomatoes can persist for several weeks or even months after harvest. Considering the susceptibility of tomatoes to damage due to their delicate and pliable nature, as well as the time lapse between harvest and demand, both manual and automated harvesting at the stage of full ripeness are not deemed optimal practices. Therefore, experimental samples were selected to include tomatoes at different stages of ripening, namely, the green-ripening stage, semi-ripening stage, and early and mid-late firm-ripening stage. During the green-ripening stage, the entire fruit is covered in green. As it enters the semi-ripening stage, the green gradually disappears, and the fruit turns orange. In the early firm-ripening stage, the fruit becomes light red with a color development rate of 6090%. Finally, in the mid-late firm-ripening stage, it turns completely red with a color rendering of nearly 100%.

2.2. Texture Analyzer

Experimental Instrument: Universal TA Texture Analyzer (Shanghai Tengba Instrument Technology Co., Ltd., Shanghai, China). Test Force Range: 0–50 kg. Test Force Accuracy: 0.0001 g. Test Speed Range: 0–50 mm/s. Test Travel Distance: 0–420 mm. Test Travel Distance Accuracy: 0.0001 mm. The software accompanying the Universal TA texture analyzer is QCTech3_A2 23.40.00.06.

2.3. Creep Test

A circular compression platen with a diameter of 100 mm was used for the probe. The creep test was configured as follows: the probe was rapidly subjected to a pre-set constant load of 5 N at the equatorial position of the fruit. The constant load was sustained for 300 s, followed by a subsequent unloading phase lasting 50 s. The return speed before and

after the test was set at 1 mm/s. The data sampling frequency of the apparatus was set to 200 points per second, which allowed for precise data collection, as shown in Figure 2. This software allows the operator to manipulate the Universal TA texture analyzer and set its experimental mode. A total of 56 tomatoes were subjected to creep tests.

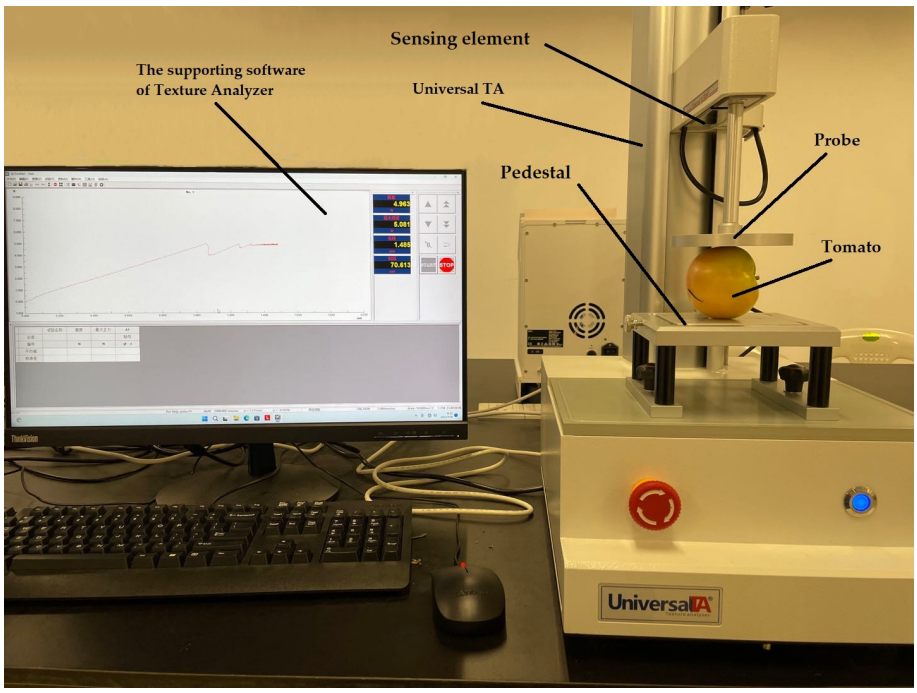


Figure 2. Universal TA texture analyzer for tomato creep test.

2.4. Puncture Test

The puncture test was conducted on three specific positions of the tomato: the first position being the septa position; the second position being the locule position; and the third position being the shoulder position, as shown in Figure 3. A total of 56 tomatoes were subjected to puncture tests.

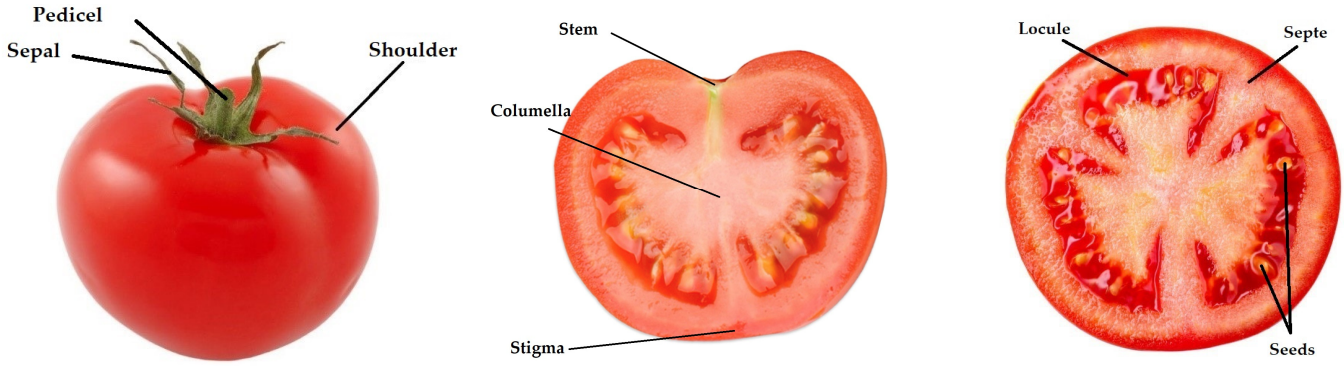


Figure 3. Anatomical map of tomato. (**a**) Whole fruit. (**b**) Longitudinal. (**c**) Cross-section.

For this test, a 2 mm needle-shaped probe was chosen, as shown in Figure 4. The compression test mode was established with a speed of 1 mm/s. Both the pre-test and post-test return velocities were maintained at 1 mm/s. The target mode, which represented the displacement of the probe, was configured to 7 mm, while the trigger force was established at 0.1 N. The instrumentation's data sampling rate was set at 200 points per second. A typical force-deformation curve was obtained as the result of the puncture test. The ratio of

the first peak force value to its displacement is defined as the exocarp brittleness (N mm^{-1}). The product of these two values divided by 2 is defined as the exocarp toughness (N mm).

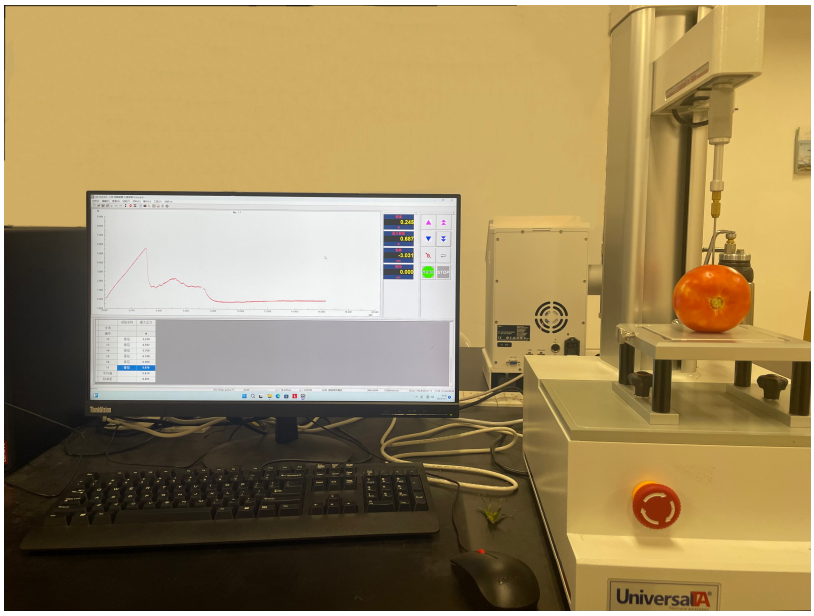


Figure 4. Puncture test.

2.5. Compression Test

This experiment utilized a circular compression platen with a diameter of 100 mm as the probe. The testing approach was configured in custom mode. Both pre-test and post-test return velocities were set at 1 mm/s. Distinct modes were applied for the radial and axial compression experiments. The target mode for displacement was set to 25 mm for radial compression, while for axial compression, it was defined at 20 mm. While tomatoes in the green-ripening stage were harder, the target mode for displacement was set to 30 mm for radial compression and axial compression. The equipment data sampling frequency was set at 200 points per second. The force-deformation curves were obtained as the result of the compression test. A total of 56 tomatoes were subjected to compression tests, of which 28 tomatoes were subjected to axial compression tests and 28 tomatoes were subjected to radial compression tests.

2.6. Creep Model

The deformation-time curve obtained from the creep test can be elucidated using various creep models, such as the Maxwell model, Kelvin model, and Burgers model. The Burgers model stands out as a classical representation for characterizing the creep attributes of viscoelastic materials among these models, as shown in Equation (1). This model consists of a cascaded connection between a Maxwell element and a Kelvin element, forming a four-element framework. The Burgers model effectively captures the fundamental characteristics of viscoelasticity and stands as one of the most renowned models for accurately predicting material creep behavior [27]. This model has been widely embraced by numerous scholars to fit the viscoelasticity of fruits [28–33]. Therefore, in this study, the Burgers model was selected to accurately depict the creep characteristics exhibited by tomatoes during the process of creep loading.

$$D(t) = \frac{F}{E_1} + \left(\frac{F}{\eta_1}\right)t + \frac{F}{E_2}\left(1 - e^{-t\frac{E_2}{\eta_2}}\right) \quad (1)$$

where $D(t)$ denotes the deformation with the unit of mm; F denotes the contact force with the unit of N; E_1 denotes the coefficient of instantaneous elasticity with the unit of N mm^{-1};

E_2 denotes the coefficient of retarded elasticity with the unit of N mm^{-1}; η_1 denotes the coefficient of serial viscosity coefficient with the unit of N s mm^{-1}; η_2 denotes the coefficient of parallel viscosity coefficient with the unit of N s mm^{-1}, and t denotes the time of the static loading with the unit of s.

After the completion of the creep test, the creep test data simplified by IBM SPSS Statistics 27 software were imported into Origin 2022. Subsequently, a line plot was generated from the data, followed by the application of nonlinear curve fitting. Create a new category named "Creep Experiment", create a function, choose the function type as Lab Talk, set the function model as explicit, and fill in the independent variable "t", dependent variable "y", and parameter settings "F", "E_1", "E_2", "η_1", and "η_2". Input the function body as "(F/E_1) + (F/η_1) * t + (F/E_2) * (1 − exp(−(E_2/η_2) * t)) + Creep Correction", set the initial value of "F" to 5 N, and check the box for fixing it. All other settings are left at their default values. Click on "Fit" to initiate the fitting process. The fitted curve, as well as the associated parameters, will be calculated by this process.

2.7. Statistical Analysis

To conduct the statistical analysis, the average value of the measured data was obtained. Variance analysis was performed using IBM SPSS Statistics 27 for Windows at a 5% significance level by using Duncan's Multiple Range Test. To study the relationships between various parameters, mechanical properties, and ripening stages, the Pearson correlation matrix method was used. The viscoelastic parameters of the creep model for tomato samples and the coefficient of determination were obtained by performing nonlinear curve fitting using Origin 2022.

3. Results and Discussion

3.1. Creep Test

As shown in Figure 5, during this experiment, the following sequence of events took place: The tomato was rapidly loaded to a predetermined constant load, resulting in an instantaneous initial deformation of the tomato. The probe was held for 300 s, which constituted the creep phase. During this phase, the tomato underwent a gradual deformation. The instrument commenced unloading after 300 s. Following unloading, the tomato pulp exhibited a noticeable recovery in deformation within a time frame of 0 to 10 s. Then, a slow recovery began. The deformation subsequently reached a state of stabilization over time, indicating the presence of permanent deformation. The occurrence of permanent deformation in the tomato under applied force indicates that plastic deformation takes place, resulting in irreversible changes. This portion induces creep-induced damage to the tomato pulp.

The creep curves of tomatoes at four different ripening stages were fitted with the nonlinear fitting function of Origin 2022. The outcomes of the fitting process notably revealed that the coefficient of determination (R^2) surpassed 0.99 for all fittings, confirming the efficacy of the selected model. Similar conclusions were found in the study by Tao et al. [34]. The shape of the creep behavior curve is profoundly influenced by the developmental stage of tomatoes, as illustrated in Figure 6. With the increase in ripeness, the creep characteristics of tomatoes changed noticeably, and the initial deformation, creep deformation, and permanent deformation of tomatoes increased correspondingly. The relationship between tomato creep deformation and permanent deformation with ripeness can be described as follows: the mid-late firm-ripening stage exhibits a higher level of deformation compared to the early firm-ripening stage, followed by the semi-ripening stage, and finally, the green-ripening stage. It showed that the firmness of tomato decreased with the increase in ripeness. This phenomenon is attributed to the increased concentration of insoluble pectin present in less ripe tomatoes, resulting in a more rigid and less malleable tissue structure. The degradation of insoluble pectin occurs during tomato ripening, resulting in the formation of soluble pectin. This transformation imparts a softening effect on the fruit, rendering it more resilient and prone to deformation as well as mechanical damage

when subjected to identical external forces. Table 2 shows the creep-fitting parameters for the four random creep-fitting curves in four ripening stages. The experimental results differed from those of Zhang et al. [14]. In Zhang et al.'s creep experiments, they derived mean values of four creep parameters (E_1, E_2, η_1, η_2) for early red-ripening stage and middle red-ripening stage fruit tomato as 4.11 N mm^{-1}, 12.29 N mm^{-1}, 1075.41 N s mm^{-1}, 77.41 N s mm^{-1}, 3.19 N mm^{-1}, 10.74 N mm^{-1}, 869.16 N s mm^{-1}, and 65.58 N s mm^{-1}. It shows that differences in tomato varieties lead to large differences in creep parameters.

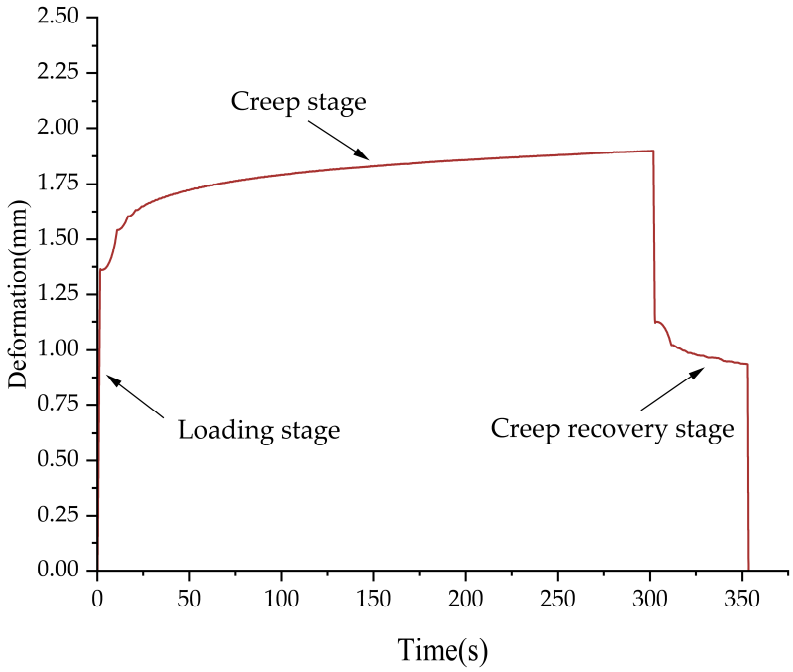


Figure 5. Creep curve of a random tomato.

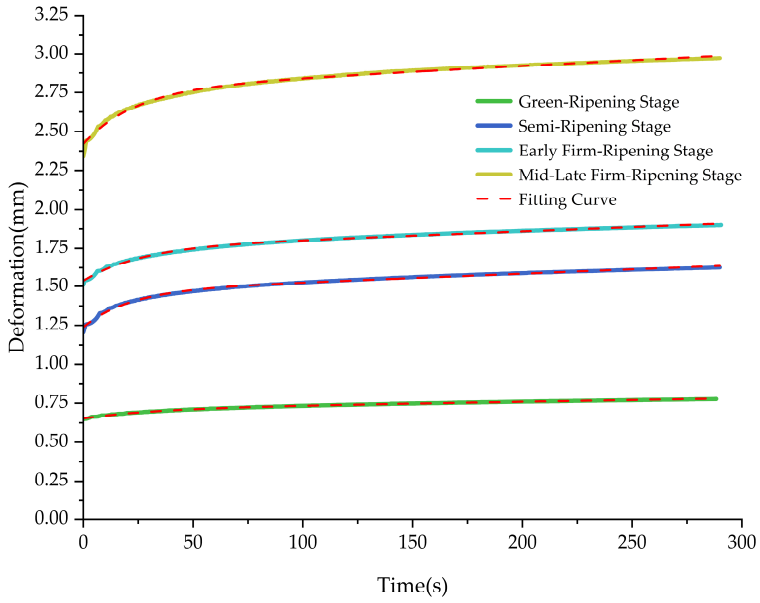


Figure 6. The four random creep-fitting curves come from four ripening stages.

Table 2. Creep-fitting parameters for the four random creep-fitting curves.

Ripening Stage	E_1/(N mm^{-1})	E_2/(N mm^{-1})	η_1/(N s mm^{-1})	η_2/(N s mm^{-1})	R^2
Green-Ripening Stage	1194.23	81.90	21808.45	2663.27	0.998
Semi-Ripening Stage	151.30	21.79	8568.42	454.63	0.996
Early Firm-Ripening Stage	183.84	23.44	9271.09	587.88	0.996
Mid-Late Firm-Ripening Stage	61.21	14.37	6607.71	342.90	0.994

The data presented in Table 2 and Figure 7 conspicuously illustrate that the four parameters corresponding to the green-ripening stage consistently exhibit larger values compared to those observed across the other three mature stages. To elucidate the relationship between each parameter and creep deformation, the ripening stages, a correlation analysis was performed. The results (Table 3) of this analysis revealed that inter-parameter correlations were identified, exhibiting an extremely high level of statistical significance ($p < 0.01$).

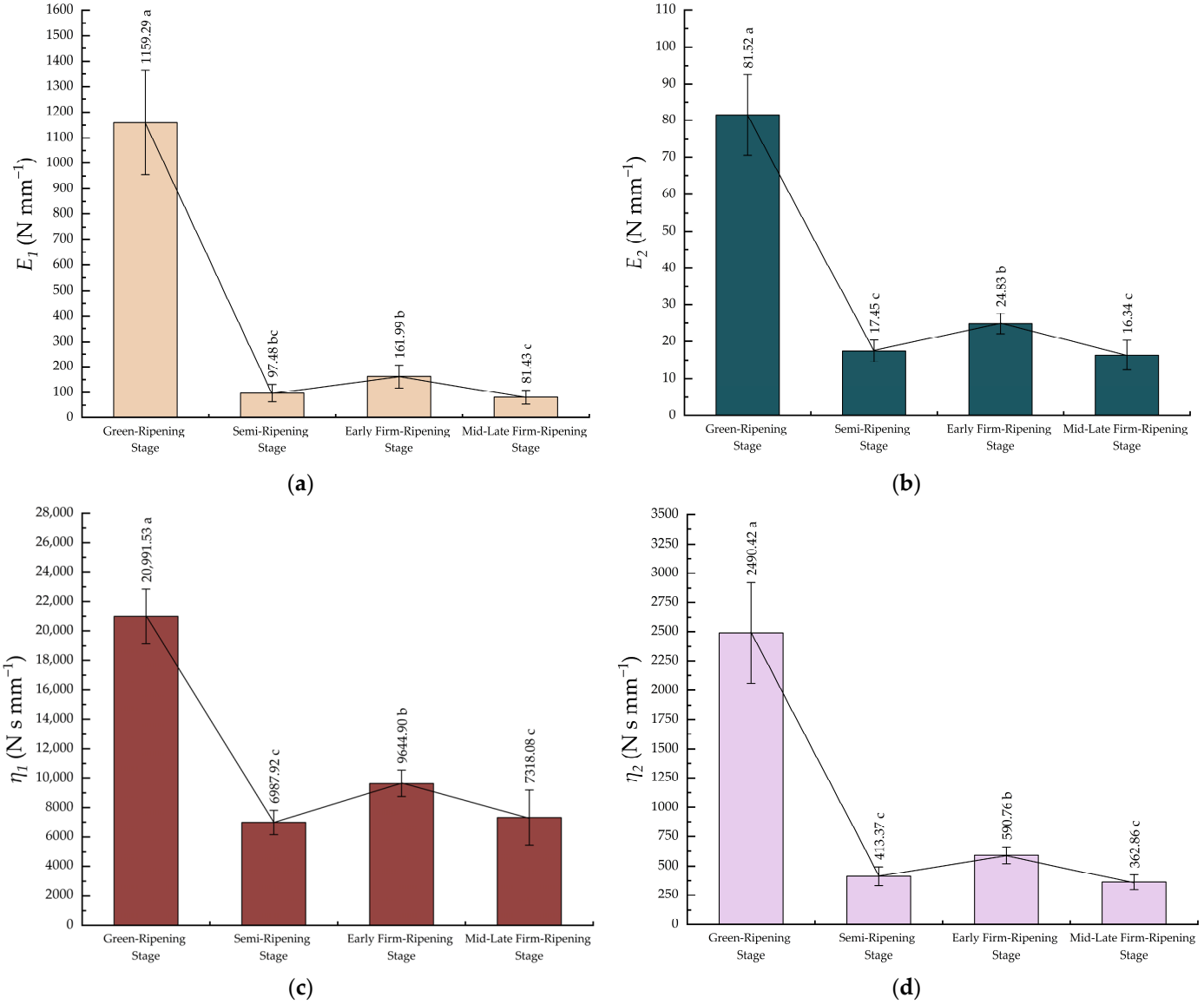


Figure 7. The average of each four parameters in the creep curve. (**a**) Parameter E_1. (**b**) Parameter E_2. (**c**) Parameter η_1. (**d**) Parameter η_2. Note: Values with different letters are significantly different according to the Duncan's multiple range test at 5% probability level.

Table 3. Correlation analysis of creep parameters.

	Ripening Stage	E_1	E_2	η_1	η_2	End Value	Start Value	Change Value
Ripening Stage	1	−0.674 **	−0.666 **	−0.617 **	−0.674 **	0.584 **	0.580 **	0.559 **
E_1		1	0.971 **	0.945 **	0.958 **	−0.819 **	−0.805 **	−0.808 **
E_2			1	0.980 **	0.995 **	−0.850 **	−0.830 **	−0.856 **
η_1				1	0.969 **	−0.892 **	−0.870 **	−0.902 **
η_2					1	−0.821 **	−0.803 **	−0.822 **
End value						1	0.995 **	0.953 **
Start value							1	0.917 **
Change value								1

Note: ** Correlation is significant at 1% probability level.

The results depicted in Figure 7 reveal a discernible trend: as tomatoes progress from the green-ripening stage to the semi-ripening stage, a conspicuous decrease in all parameter values becomes evident. The transition from the semi-ripening stage to the early firm-ripening stage was accompanied by a slight increase in parameter values. A plausible explanation for this disparity could be attributed to the fact that the average creep deformation value during the semi-ripening stage surpasses that of the early firm-ripening stage within the experimental samples. According to the correlation analysis between the creep variable and the ripening stages, as well as the four parameters (Table 3), the Pearson correlation coefficient between the four parameters and ripening stages ranges from 0.6 to 0.7, while the Pearson correlation coefficient between the four parameters and the start, end, and change values, ranges from 0.8 to 1.0. The shape variable, rather than the ripening period, is found to have a direct correlation effect on four parameters. There are obvious individual differences in fruits, and the situation of high ripening and low creep deformation variables will appear. Therefore, the hardness of the tomato cannot be directly judged by the ripening stage.

The viscoelastic parameters obtained from these experiments could effectively inform the force control strategy employed by harvesting robots. The experimentally obtained creep equation can be transformed into the Prony series describing the viscoelasticity of tomato. Using ANSYS, a finite element model of the tomato can be developed to simulate the deformation and contact force generated when the end-effector grips the tomato. Thus, the picking force is optimized to ensure picking stability and fruit integrity [35].

3.2. Puncture Test

The force-displacement curves of exocarp rupture for a tomato sample at the semi-ripening stage, obtained from both the septa and locule positions, are depicted in Figure 8. The curve visually illustrates the complete process of gradual penetration of the needle-shaped probe of the texture analyzer from the tomato's exocarp into its pulp.

During the penetration of the tomato's exocarp, a gradual increase in the applied force by the probe was observed. Initially, an initial peak force was observed, indicating the rupture force of the outer exocarp. Notably, no distinct peak was observed after the probe traversed through the exocarp during punctures conducted at the septa position. However, in cases of puncturing at the locule position, a distinct secondary peak emerges subsequent to successful exocarp penetration by the probe. The second peak was attributed to the probe penetrating through the endocarp, with the rupture force of the endocarp corresponding to the value of the second peak.

The force value at the first peak corresponds to the rupture force, i.e., exocarp rupture force (N). The displacement at the first peak represents the exocarp rupture depth (mm). The ratio of the first peak force value to its displacement is defined as the exocarp brittleness (N mm^{-1}). The product of these two values is defined as the exocarp toughness (N mm). Table 4 below presents the exocarp rupture force, exocarp rupture depth, exocarp brittleness, and exocarp toughness for different ripening stages. Mechanical parameters were found to be different at a 5% probability level for all the ripening stages.

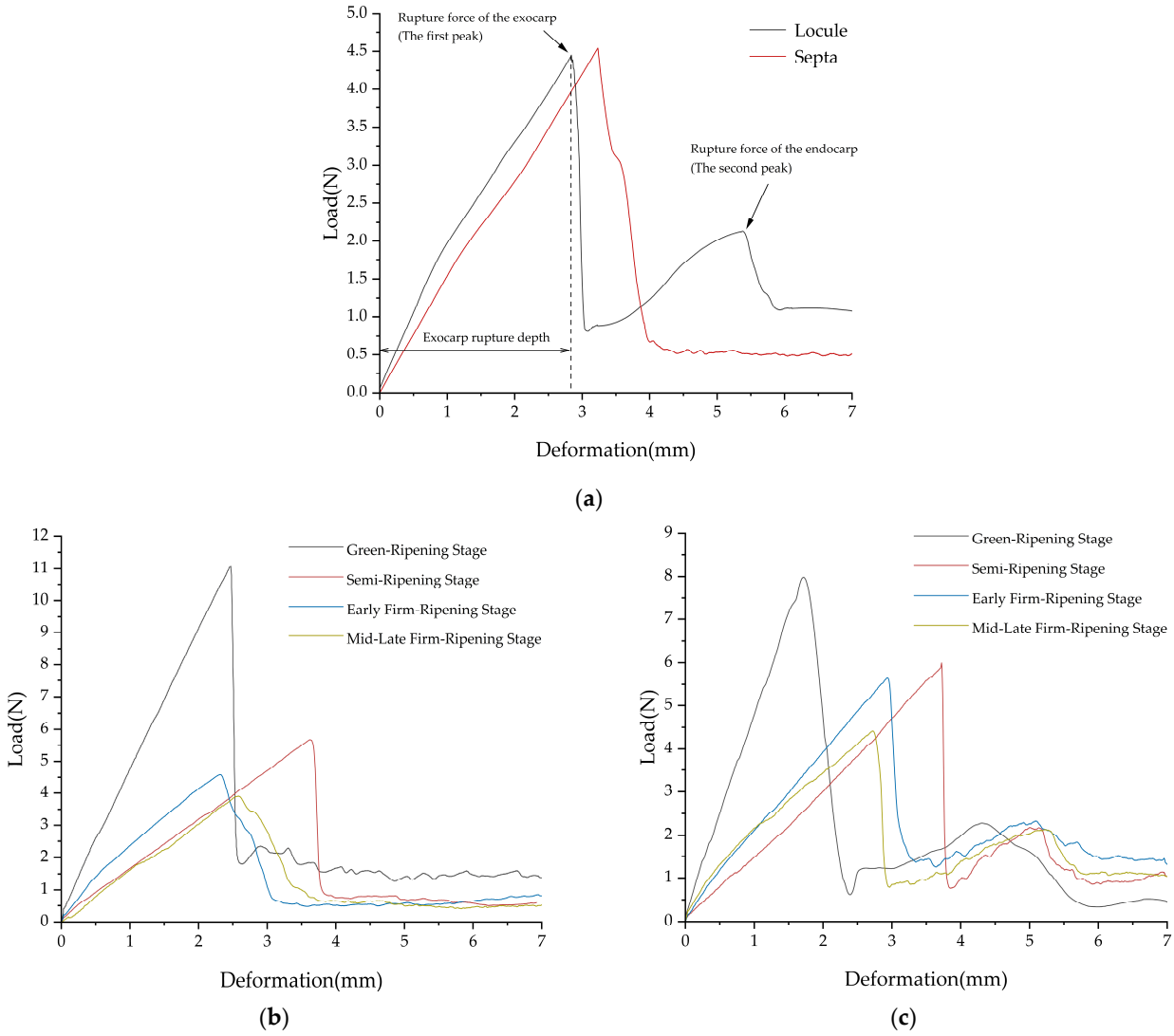


Figure 8. The force-deformation curve for puncture tests. (**a**) Puncture curves at two different locations. (**b**) Septa position puncture curves of tomato at four different ripening stages. (**c**) Locule position puncture curves of tomato at four different ripening stages.

Table 4. Exocarp rupture force, exocarp rupture depth, exocarp brittleness, and exocarp toughness at different ripening stages.

Ripening Stage	Experimental Results	Exocarp Rupture Force/(N)	Exocarp Rupture Depth/(mm)	Exocarp Brittleness/ (N mm^{-1})	Exocarp Toughness/ (N mm)
Green-Ripening Stage	Max	11.476	3.534	5.745	20.280
	Mean	9.224 ± 0.901 a	2.016 ± 0.359 d	4.657 ± 0.621 a	9.384 ± 2.439 b
	Min	7.415	1.488	3.247	5.634
Semi-Ripening Stage	Max	7.651	5.157	2.604	19.314
	Mean	5.996 ± 0.952 b	3.471 ± 0.730 b	1.770 ± 0.328 c	10.598 ± 3.415 a
	Min	3.982	2.223	1.123	5.242
Early Firm-Ripening Stage	Max	6.807	4.327	2.798	12.776
	Mean	5.408 ± 0.688 c	2.822 ± 0.590 c	1.974 ± 0.359 b	7.717 ± 2.163 c
	Min	3.884	1.668	1.349	3.239
Mid-Late Firm-Ripening Stage	Max	6.415	5.697	1.769	16.258
	Mean	4.521 ± 0.654 d	3.781 ± 0.758 a	1.229 ± 0.239 d	8.651 ± 2.640 bc
	Min	3.315	2.657	0.855	5.230

Note: Values with different letters are significantly different according to the Duncan's multiple range test at 5% probability level.

By conducting correlation analysis, we investigated the relationship between the ripening stage and mechanical parameters, including exocarp rupture force, exocarp rupture depth, and exocarp brittleness. The results revealed significant correlations ($p < 0.01$) between the ripening stage and these mechanical attributes. The Pearson correlation coefficients were calculated to be 0.854, 0.603, and 0.852 for exocarp rupture force, exocarp rupture depth, and exocarp brittleness, respectively.

As illustrated in Figure 9, a variation in exocarp rupture forces was observed among tomatoes at different stages of ripening. The exocarp rupture force decreases during maturity. Similar results have also been reported by Bui et al. [36]. The average exocarp rupture force for the semi-ripening stage was 5.996 ± 0.952 N, whereas for the early firm-ripening stage and mid-late firm-ripening stage, the corresponding values were 5.408 ± 0.688 N and 4.521 ± 0.654 N, respectively. The average peel rupture force during the green-ripening stage was 9.224 ± 0.901 N, which was 53.87% higher than that during the semi-ripening stage, 70.63% higher than that during the early firm-ripening stage, and 104.01% higher than during the mid-late firm-ripeness stage. The experimental results differed from those of Ince et al. [13]. In the puncture experiment of Ince et al., the mean puncture rupture force of the green tomato was 6.920 N; the mean puncture rupture force of the pink tomato was 3.986 N, and the mean puncture rupture force of the red tomato was 2.735 N. The mean rupture force of the various stages of the present experiment was greater than that of the experimental results of Ince et al. However, the puncture force of green tomato was 151.82% higher than that of red tomato in Ince et al. [13] humanities, and the green-ripening stage was 104% higher than that of the mid-late firm-ripeness stage in this paper, and both results indicated that there was a significant decrease in the rupture force from the green-ripening stage to firm ripening stage. The average hardness in the puncture test results of Ince et al. were 4.1225, 1.5548, and 1.1053 (N mm^{-1}), respectively, and these test results were not significantly different from those of this paper. The exocarp toughness in this paper is different from the experimental results of Ince et al. and Sirisomboon et al. [37]. In this paper, the highest exocarp toughness was found in tomatoes at the semi-ripening stage, whereas green tomatoes had the highest exocarp toughness in the results of the study by Ince et al. and Sirisomboon et al.

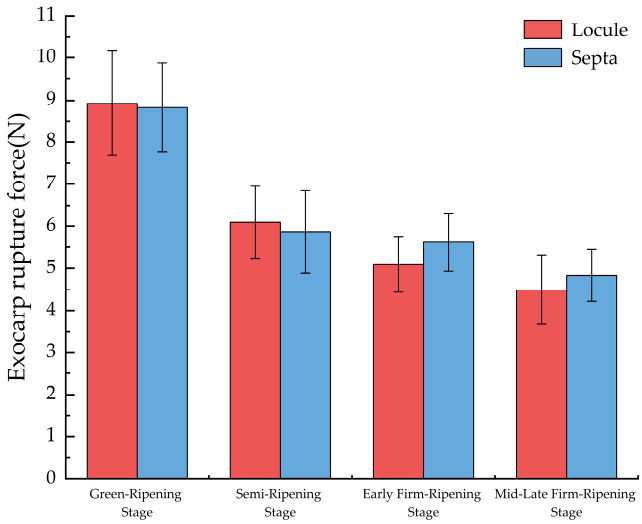


Figure 9. Average exocarp rupture force at different ripening stages.

It indicates that there is a significant difference in the parameter values of mechanical properties depending on the tomato variety. Similar conclusions were found in the study by Vieira et al. [38].

The impact of ripening stages on exocarp rupture force in both the locule and septa positions of tomatoes was assessed through correlation analysis. These results demonstrate a significant impact of the ripening stage on exocarp rupture force ($p < 0.01$), accompa-

nied by a strong Pearson correlation coefficient of 0.884, indicating a robust association. Additionally, a parallel analysis was conducted to investigate the correlation between the rupture force of exocarp and puncture locations at various sites. The Pearson correlation coefficient was 0.404, and the results indicated a moderate statistical correlation ($p < 0.05$).

The results presented in Figure 10 clearly demonstrate that among tomatoes at the same ripening stage, while locule and septa were statistically within the same group for exocarp rupture force values, the shoulder showed the difference. The exocarp rupture force was significantly higher in the shoulder region compared to the equatorial region. This disparity could be attributed to the inherent maturation process of tomatoes, whereby ripening is initiated from the stigma end and advanced toward the shoulder. The shoulder region demonstrates a higher level of resistance to puncture. In the context of automated tomato harvesting robots, the failure to adequately trim tomato pedicels can engender potential complications. Specifically, during the transportation phase, semi-ripening stage, and firm-ripening stage, tomatoes possessing untrimmed pedicels might puncture neighboring tomato fruits, culminating in the rupture of their exocarp or even their peel. Such occurrences could result in compromised fruit quality or, in more severe instances, lead to spoilage. It was also emphasized in the study of Desmet et al. [39] that stems that have been left unpruned after tomatoes have been picked could cause puncture wounds to the rest of the tomatoes. So, when picking tomatoes after the green-ripening stage, it is necessary to pay attention to the pruning of the fruit pedicel, which can be pruned at the same time as picking and also can increase the process of pruning the fruit pedicel after picking. This requires that when designing the end-effector, it should be able to prune the pedicel completely when picking. Alternatively, employ specialized packaging patterns during the packaging procedure to mitigate the risk of stalks puncturing the tomatoes.

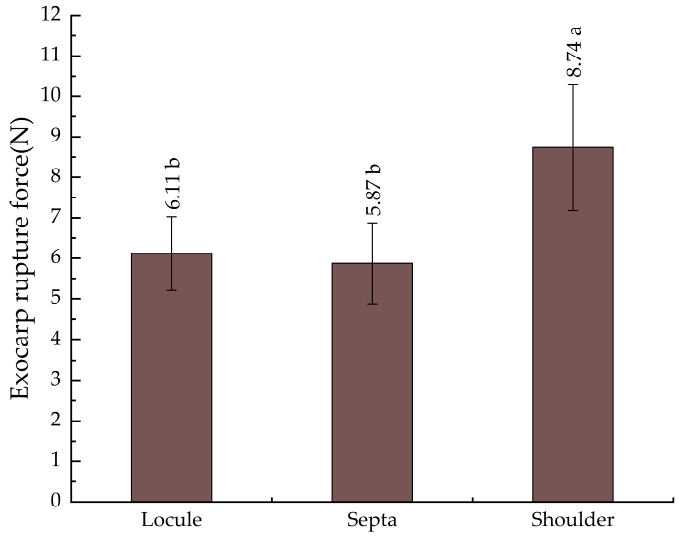


Figure 10. Average exocarp rupture force comparison between shoulder and equator locations. Note: Values with different letters are significantly different according to the Duncan's multiple range test at 5% probability level.

3.3. Compression Test

Figure 11 illustrates the radial compression profiles of tomatoes at four distinct stages of ripening. The compression progression unfolded through three phases. During the initial phase, as the force was incrementally applied through the flat plate probe, there was a corresponding increase in the force exerted on the tomato's surface, resulting in a concurrent elevation in deformation. During this phase, the correlation between load and deformation maintained an approximate linearity, which is indicative of elastic compression.

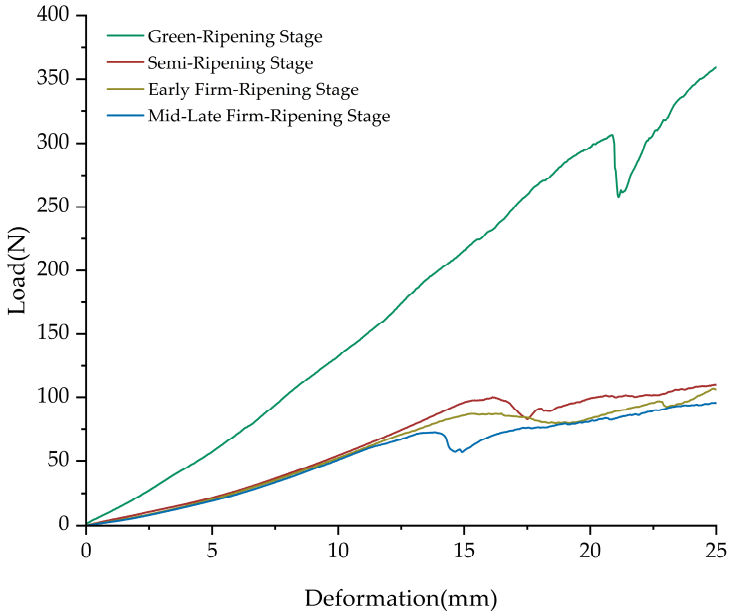


Figure 11. Radial compression curves of tomato at four ripening stages.

During the subsequent phase, as the application of load persists, the previously linear association between load and deformation becomes disrupted, and the tomato initiates the process of rupture. Initially, minute radial cracks emerge, primarily originating from the stem end. These cracks gradually propagate as the applied load intensifies. This progressive crack propagation culminates in complete rupture, commencing from the stem end and culminating in a reduction in the fruit's capacity to counter deformation, attributable to the inflicted impairment on the integrity of the fruit's pulp tissue.

In the third phase of the compression process, after the rupture of the exocarp, the application of additional load engendered a continuous compression of the fruit's pulp. This sequential compression resulted in a persistent ascent of the load-deformation curve. Notably, no discernible biological yield point existed throughout this compression phase. The initial peak observed in the curve corresponded to the point at which rupture occurred in the tomato's exocarp, indicating the initiation of exocarp rupture. Under axial loading conditions, diminutive cracks emerged along the axial orientation of the exocarp when the applied load reached its maximum rupture force. These cracks progressively expanded until culminating in a complete rupture. The locations of the observed crack occurrences are consistent with the observations of Xiong et al. [40] and Liu et al. [41].

The results in Figure 12 and Table 5 show that regardless of the axial and radial loading conditions, the deformation of tomatoes at the point of dehiscence was close for the three ripening stages except for the green-ripening stage; however, there is a significant disparity in terms of extrusion rupture force. From Table 5, it can be observed that under radial loading, the average rupture force follows the following relationships: green-ripening > semi-ripening stage > early firm-ripening stage > mid-late firm-ripening stage. In the context of axial loading, the average rupture force follows this sequence: green-ripening stage > early firm-ripening stage > semi-ripening stage > mid-late firm-ripening stage. The extrusion resistance of different tomatoes was found to vary significantly, even within the same ripening period. The axially averaged rupture forces obtained in this experiment for tomatoes at the semi-ripening stage were close to those of Liu et al. [41], but there was a difference in the rupture force at the green-ripening stage. It is important to acknowledge that certain weaker semi-ripening fruits may exhibit compressive rupture forces even lower than those observed for more robust early firm-ripening stage and mid-late firm-ripening stage fruits.

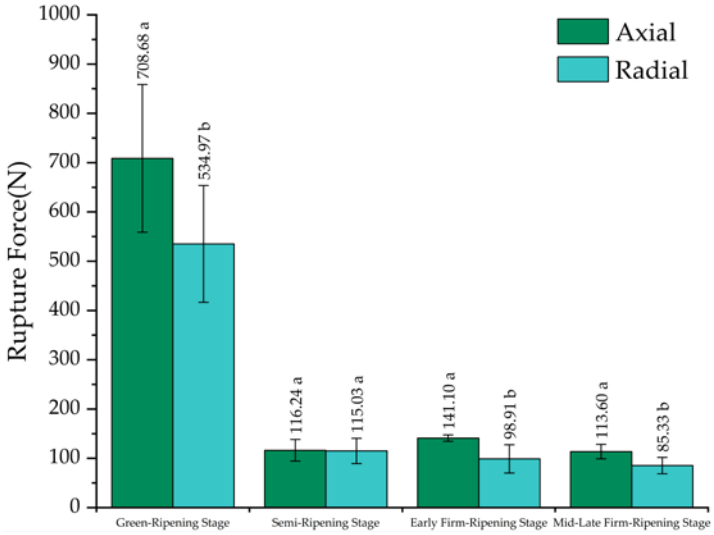


Figure 12. Average rupture force in different compression directions for four ripening stages. Note: Values with different letters are significantly different according to the Duncan multiple range test at 5% probability level.

Table 5. Tomato fruit compression rupture force and rupture deformation.

Loading Direction	Experimental Results	Green-Ripening Stage		Semi-Ripening Stage		Early Firm-Ripening Stage		Mid-Late Firm-Ripening Stage	
		Rupture Force/(N)	Rupture Deformation/(mm)	Rupture Force/(N)	Rupture Deformation/(mm)	Rupture Force/(N)	Rupture Deformation/(mm)	Rupture Force/(N)	Rupture Deformation/(mm)
Axial	Max	991.30	29.72	143.11	16.93	148.72	16.78	136.74	18.74
	Mean	708.68 ± 149.89 a	24.70 ± 2.99	116.24 ± 21.90 a	15.03 ± 1.84	141.10 ± 6.41 a	14.80 ± 1.81	113.60 ± 14.72 a	14.49 ± 2.48
	Min	540.34	20.44	84.94	11.91	131.12	12.09	99.56	12.32
Radial	Max	790.41	28.14	151.37	20.26	148.04	20.94	106.23	18.86
	Mean	534.97 ± 118.52 b	24.19 ± 4.16	109.71 ± 24.75 b	16.86 ± 3.04	98.91 ± 28.65 b	17.04 ± 3.02	85.33 ± 16.54 b	16.30 ± 2.69
	Min	306.21	13.63	81.22	12.03	52.67	12.09	62.13	12.49

Note: Values with different letters are significantly different according to the Duncan multiple range test at 5% probability level.

The internal architecture of the fruit exhibits a structural resemblance to that of a wheel, wherein the mesocarp, septa, and columella correspond to the rim, spokes, and hub, respectively. From the green fruit stage to the green-ripening stage, the internal structure of the fruit is gradually developed and complete, and the bearing capacity of the wheel structure reaches the maximum. With the increase in maturity, the columella and septa of the fruit are constantly fluidizing, and the spoke and hub functions in the wheel structure disappear rapidly. Moreover, the mesocarp concurrently undergoes a softening phenomenon, leading to an uninterrupted reduction in the fruit's load-bearing capability [10].

As illustrated in Figure 12 and detailed in Table 5, the axial and radial compressive rupture forces in the green-ripening, early firm-ripening stage, and mid-late firm-ripening stage were found to be different at 5% probability level, and when assessing tomatoes at the same stage of ripeness, the axial compressive rupture force exceeds the radial rupture force. When these fruits are subjected to both axial and radial compression, their columella undergoes compression and tension, respectively. Due to its viscoelastic composition, columella demonstrates a significantly higher compressive strength compared to its tensile strength. Therefore, the axial compression resistance of tomatoes is obviously greater than that of the radial resistance. The same conclusion was reached by Xiong et al. [40] and Liu et al. [41]. These outcomes accentuate the inherent anisotropic characteristics of tomatoes. In the current design of tomato harvesting robots, the predominant approach involves employing radial gripping techniques. In future iterations of robot design, particularly in scenarios requiring increased gripping forces, axial gripping may be a new design direction to mitigate potential damage to tomatoes.

4. Conclusions

The tomato cultivar Syngenta Sibede was utilized as the experimental material, and a four-element Burgers model was employed to approximate the viscoelastic behavior and deformation characteristics of tomatoes through creep testing. The fitting coefficients exceeded 0.99. By employing this modeling approach, we obtained the creep parameters for each of the four distinct ripening stages. A comprehensive analysis was undertaken to discern the correlation between the ripening stage, deformation value, and these identified creep parameters. The test results show that the Pearson correlation coefficient between the four parameters and the ripening stage ranges from 0.6 to 0.7 ($p < 0.01$), while the Pearson correlation coefficient between the four parameters and the start, end, and change values ranges from 0.8 to 1.0 ($p < 0.01$), and it revealed that inter-parameter correlations were identified, exhibiting an extremely high level of statistical significance ($p < 0.01$). The viscoelastic parameters obtained from these experiments could effectively inform the force control strategy employed by harvesting robots.

Transitioning to the puncture test, a crucial component of this study, revealed that the average exocarp rupture force for tomatoes at the semi-ripening stage was determined to be 5.996 ± 0.952 N. The corresponding values for the early firm-ripening stage and mid-late firm-ripening stage were 5.408 ± 0.688 N and 4.521 ± 0.654 N, respectively. The observed trend suggests a slight increase in the peel rupture force from the early firm-ripening stage to the semi-ripening stage. Notably, the green-ripening stage exhibited a significantly higher exocarp rupture force of 9.224 ± 0.901 N, indicating a remarkable increase of 53.87%, 70.63%, and 104.01% compared to the semi-ripening stage, early firm-ripening stage, and mid-late firm-ripening stage, respectively. The experimental results have demonstrated the importance of fruit pedicel pruning, particularly when harvesting tomatoes during the semi-ripening stage and beyond.

Results garnered from the compression test elucidated a notable discrepancy between axial and radial compressive rupture forces within the same ripening stage. It means that tomatoes are anisotropic. The results of this experiment also showed that the stem of the tomato is the weak part. In the current design of tomato harvesting robots, the predominant approach involves employing radial gripping techniques. In future iterations of robot design, particularly in scenarios requiring increased gripping forces, axial gripping may be a strategic approach to mitigate potential damage to tomatoes. In comparison with the experimental results of previous scholars, it was found that the mechanical properties of tomatoes differed greatly from one variety to another.

Author Contributions: Conceptualization, M.H.; methodology, M.H., X.J. and X.W.; software, M.H.; validation, X.J. and Z.Z.; formal analysis, M.H.; investigation, Z.Z. and X.J.; resources, M.H., X.J. and Z.Z.; data curation, M.H. and X.W.; writing—original draft preparation, M.H.; writing—review and editing, S.Z. and W.W.; visualization, M.H., X.W. and W.W.; project administration, W.W. and S.Z.; funding acquisition, S.Z. All authors have read and agreed to the published version of the manuscript.

Funding: This work was supported by the Guiding Project of the Fujian Provincial Department of Science and Technology (grant number 2022N0009) and the Cross-Disciplinary Project of Fujian Agriculture and Forestry University (grant number 000-71202103B).

Institutional Review Board Statement: Not applicable.

Informed Consent Statement: Not applicable.

Data Availability Statement: All data are presented in this article in the form of figures and tables.

Acknowledgments: The authors would like to acknowledge the College of Mechanical Electronic Engineering, Fujian Agriculture and Forestry University.

Conflicts of Interest: The authors declare no conflict of interest.

References

1. Sun, Y.Z.; He, J.; Wei, F. Development and International Competitiveness Evaluation of China's Tomato Industry in the 13th Five-Year Plan Period. *Zhongguo Gua-Cai* **2023**, *36*, 112–116.
2. Zhang, J.; Liu, S.; Zhu, X.; Chang, Y.; Wang, C.; Ma, N.; Wang, J.; Zhang, X.; Lyu, J.; Xie, J. A Comprehensive Evaluation of Tomato Fruit Quality and Identification of Volatile Compounds. *Plants* **2023**, *12*, 2947. [CrossRef]
3. Malik, M.; Zhang, T.; Li, H. Mature Tomato Fruit Detection Algorithm Based on improved HSV and Watershed Algorithm. In Proceedings of the 6th International Federation of Automatic Control (IFAC) Conference on Bio-Robotics (BIOROBOTICS), Beijing, China, 13–15 July 2018.
4. Wang, P.C. Research on Tomato Fruit Growth Pose Recognition and Harvesting Control Based on Binocular Vision. Ph.D. Thesis, Zhejiang Sci-Tech University, Hangzhou, China, 1 May 2021.
5. Samuel, D.V.K. Manually operated tomato harvesting tool for greenhouse. *Acta Hortic.* **2006**, *710*, 491–496. [CrossRef]
6. Evans, W.; Cerven, V.; Winter, N.; Coker, C. A Proposed Alternative Production Regime for Cherry and Grape Tomato Using Compact Plants and Once-over Harvest. *HortTechnology* **2010**, *20*, 620–622. [CrossRef]
7. Yang, Z.; Amin, A.; Zhang, Y.; Wang, X.; Chen, G.; Abdelhamid, M.A. Design of a Tomato Sorting Device Based on the Multisine-FSR Composite Measurement. *Agronomy* **2023**, *13*, 1778. [CrossRef]
8. Tsai, C.; Kao, I.; Shibata, A.; Yoshimoto, K.; Higashimori, M.; Kaneko, M. Experimental study of creep response of viscoelastic contact interface under force control. In Proceedings of the International Conference on Intelligent Robots and Systems, Taipei, China, 18–22 October 2010.
9. Deng, Y.; Wu, Y.; Li, Y.F. Biomechanical Characteristics and Texture Detection of Fruits and Vegetables During Storage and Transportation. *Trans. Chin. Soc. Agric. Eng.* **2005**, *21*, 1–6.
10. Li, Z.G. Research on Grasping Damage of Tomato Harvesting Robot Based on Tomato Biomechanical Characteristics. Ph.D. Thesis, Jiangsu University, Zhenjiang, China, 15 June 2011.
11. Zhou, J.; Zhang, N.; Meng, Y.; Wang, M. Online Estimation of Tomato Viscoelastic Parameters for Robot Grasping. *Nongye Jixie Xuebao* **2017**, *48*, 26–32.
12. Wang, B.; Zhang, W.; Feng, Q. Measurement and Analysis of Stem-Clamping Mechanical Properties for Automatic Pruning of Tomatoes. *J. Agric. Mech. Res.* **2023**, *45*, 157–163.
13. Ince, A.; Cevik, M.Y.; Vursavuş, K.K. Effects of Ripening Stages on Textural Mechanical Properties of Tomato. *Int. J. Agric. Biol. Eng.* **2016**, *9*, 200–206.
14. Zhang, B.; Zhou, J.; Meng, Y.; Zhang, N.; Gu, B.; Yan, Z.; Idris, S.I. Comparative study of mechanical damage caused by a two-finger tomato gripper with different robotic grasping patterns for harvesting robots. *Biosyst. Eng.* **2018**, *171*, 245–257. [CrossRef]
15. Pham, Q.; Liou, N. Investigating texture and mechanical properties of Asian pear flesh by compression tests. *J. Mech. Sci. Technol.* **2017**, *31*, 3671–3674. [CrossRef]
16. Stropek, Z.; Golacki, K. Quantity assessment of plastic deformation energy under impact loading conditions of selected apple cultivars. *Postharvest Biol. Tec.* **2016**, *115*, 9–17. [CrossRef]
17. Stropek, Z.; Golacki, K. Bruise susceptibility and energy dissipation analysis in pears under impact loading conditions. *Postharvest Biol. Tec.* **2020**, *163*, 111120. [CrossRef]
18. Shirvani, M.; Ghanbarian, D.; Ghasemi-Varnamkhasti, M. Measurement and evaluation of the apparent modulus of elasticity of apple based on Hooke's, Hertz's and Boussinesq's theories. *Measurement* **2014**, *54*, 133–139. [CrossRef]
19. Bi, C.; Li, D.; Wang, L.; Adhikari, B. Viscoelastic properties and fractal analysis of acid-induced SPI gels at different ionic strength. *Carbohydr. Polym.* **2013**, *92*, 98–105. [CrossRef]
20. Chen, J.; Zhao, N.; Fu, N.; Li, D.; Wang, L.; Chen, X. Mechanical Properties of Hulless Barley Stem with Different Moisture Contents. *Int. J. Food. Eng.* **2019**, *15*, 20180033. [CrossRef]
21. Hou, J.; He, Z.; Liu, D.; Zhu, Z.; Long, Z.; Yue, X.; Wang, W. Mechanical Damage Characteristics and Nondestructive Testing Techniques of Fruits: A Review. *Food Sci. Technol.* **2023**, *43*, e001823. [CrossRef]
22. Jahanbakhshi, A.; Yeganeh, R.; Shahgoli, G. Determination of Mechanical Properties of Banana Fruit under Quasi-Static Loading in Pressure, Bending, and Shearing Tests. *Int. J. Fruit Sci.* **2020**, *20*, 314–322. [CrossRef]
23. Wu, K.; Lou, J.; Li, C.; Luo, W.; Li, C.; Li, J. Creep Modelling of Rootstock during Holding in Watermelon Grafting. *Agriculture* **2021**, *11*, 1266. [CrossRef]
24. Vu, Q.; Ronzhin, A. A Model of Four-Finger Gripper with a Built-in Vacuum Suction Nozzle for Harvesting Tomatoes; Smart Innovation, Systems and Technologies. In Proceedings of the 14th International Conference on Electromechanics and Robotics "Zavalishin's Readings", Kursk, Russia, 17–20 April 2019; Spinger: Singapore, 2020; pp. 149–160.
25. Jun, J.; Kim, J.; Seol, J.; Kim, J. Towards an Efficient Tomato Harvesting Robot: 3D Perception, Manipulation, and End-Effector. *IEEE Access* **2021**, *9*, 17631–17640. [CrossRef]
26. Deimel, R.; Brock, O. A novel type of compliant and underactuated robotic hand for dexterous grasping. *Int. J. Robot. Res.* **2016**, *35*, 161–185. [CrossRef]
27. Yang, M. *Rheology of Agricultural Materials*; China Agriculture Press: Beijing, China, 2010; pp. 56–83.
28. Zhuang, M.; Li, G.; Ding, K.; Xu, G. Research on the application of impedance control in flexible grasp of picking robot. *Adv. Mech. Eng.* **2023**, *15*, 16878132231161016. [CrossRef]

29. Psarra, E.; George, C.P. Luffa Cylindrica as a Durable Biofiber Reinforcement for Epoxy Systems. *Compos. Sci. Technol.* **2021**, *203*, 108597. [CrossRef]
30. Wu, X.; Wang, C.; Guo, Y. Effects of the high-pulsed electric field pretreatment on the mechanical properties of fruits and vegetables. *J. Food. Eng.* **2020**, *274*, 109837. [CrossRef]
31. Wei, J.; Tang, C.; Xu, B.; He, G. Contact force modeling and variable damping impedance control of apple harvesting robot. *Comput. Electron. Agric.* **2022**, *198*, 107026.
32. Wei, J.; Ding, Y.; Xu, B.; Chen, G.; Zhao, D. Adaptive Variable Parameter Impedance Control for Apple Harvesting Robot Compliant Picking. *Complexity* **2020**, *2020*, 4812657. [CrossRef]
33. Quintana, S.; Llalla, O.; García-Zapateiro, L.; García-Risco, M.; Fornari, T. Preparation and Characterization of Licorice-Chitosan Coatings for Postharvest Treatment of Fresh Strawberries. *Appl. Sci.* **2020**, *10*, 8431. [CrossRef]
34. Tao, Y.; Zhou, J.; Wang, M.; Zhang, N.; Meng, Y. An optimum strategy for robotic tomato grasping based on real-time viscoelastic parameters estimation. *Int. J. Adv. Robot. Syst.* **2017**, *14*, 1–8. [CrossRef]
35. Qian, Z. Study on Grasping Model and Compliance Control of Gripper of Apple Picking Robot. Master's Thesis, Jiangsu University, Zhenjiang, China, 10 June 2019.
36. Bui, H.; Makhlouf, J.; Ratti, C. Postharvest ripening characterization of greenhouse tomatoes. *Int. J. Food Prop.* **2010**, *13*, 830–846. [CrossRef]
37. Sirisomboon, P.; Tanaka, M.; Kojima, T. Evaluation of tomato textural mechanical properties. *J. Food Eng.* **2012**, *111*, 618–624. [CrossRef]
38. Vieira, D.; Caliari, M.; Souza, E.; Soares Júnior, M. Mechanical resistance, biometric and physicochemical characteristics of tomato cultivars for industrial processing. *Food Sci. Technol.* **2019**, *39*, 363–370. [CrossRef]
39. Desmet, M.; Lammertyn, J. The relative influence of stem and fruit properties on stem puncture injury in tomatoes. *Postharvest Biol. Tec.* **2004**, *33*, 101–109. [CrossRef]
40. Xiong, Z.; Li, H.; Hou, L. Study on mechanical properties of cherry tomato for robot picking. *Mod. Agric. Equip.* **2020**, *41*, 24–28.
41. Liu, J.; Li, P.; Li, Z. Experimental study on mechanical properties of tomatoes for robotic harvesting. *Nongye Gongcheng Xuebao* **2008**, *24*, 66–70.

Disclaimer/Publisher's Note: The statements, opinions and data contained in all publications are solely those of the individual author(s) and contributor(s) and not of MDPI and/or the editor(s). MDPI and/or the editor(s) disclaim responsibility for any injury to people or property resulting from any ideas, methods, instructions or products referred to in the content.